Compression curves of transition metals in the Mbar range: Experiments and projector augmented-wave calculations

Agnès Dewaele,[1] Marc Torrent,[1] Paul Loubeyre,[1] and Mohamed Mezouar[2]
[1]*Département de Physique Théorique et Appliquée, CEA, Bruyères-le-Châtel, 91297 Arpajon Cedex, France*
[2]*European Synchrotron Radiation Facility, BP 220, F-38043 Grenoble Cedex, France*
(Received 19 May 2008; revised manuscript received 6 July 2008; published 3 September 2008)

The ambient temperature equations of state (EoS) of iron, cobalt, nickel, zinc, molybdenum, and silver have been measured by x-ray diffraction. These transition metals were compressed using diamond anvil cells with a helium pressure transmitting medium. The maximum pressure reached during these experiments varied between 65 GPa (for cobalt) and 200 GPa (for iron). This work completes previous measurements on six other metals [Phys. Rev. B **70**, 094112 (2004)] to quantify the differences between *ab initio* calculations and experiment on a large experimental set of transition metals. The compression curves of iron, cobalt, nickel, zinc, molybdenum, silver, platinum, and gold are also calculated *ab initio* within the density-functional theory (DFT) formalism using the projector augmented-wave (PAW) method and different exchange-correlation functionals (LDA, GGA-PBE, GGA-PBEsol). The difference between PAW and available all-electron calculations is found to be negligible up to very high pressures. The success of each exchange-correlation functional is correlated with the atomic number. For all metals, the bulk modulus becomes overestimated at high pressure. In addition, this extended data set of metals' EoS enables to reduce further, but marginally, the systematic uncertainty of the high-pressure metrology based on the ruby standard.

DOI: 10.1103/PhysRevB.78.104102 PACS number(s): 64.30.−t, 07.35.+k, 71.15.Nc

I. INTRODUCTION

The equation of state is perhaps the most fundamental property of condensed matter. Many properties of a material are determined from it. It is also an essential input to model earth and planetary interiors[1] or to hydro-code simulate dynamical processes, such as inertial confinement fusion.[2] In the past decade, great progress in the accuracy of the determination of the cold compression curve has been achieved, either with static experiments up to the 200 GPa range or with the *ab initio* calculations of the ground electronic state. In a previous series of measurements on six metals, Al, Cu, Ta, W, Pt, and Au,[3] state-of-the-art accuracy of the volume determination has been used to revisit the ruby pressure scale calibration and thus reduce the associated systematic uncertainty of the equation of state measurements. *Ab initio* calculations are especially valuable to simulate conditions for which experiments are difficult or impossible. The aim of this paper is to quantify the biases and to disclose systematic trends of these calculations at high pressure on a significant set of transition metals. To cite Martin:[4] "Comparison of theory and experiment is one of the touchstones of *ab initio* electronic structure research. Because direct comparison can be made with experiment, the equation of state is one of the tests of the state of the theory, in particular, the approximations made to treat electron-electron interactions."

We present here a joined theoretical and experimental determination of the equations of state (EoS) of several transition metals: Fe (Z=26; $[Ar]3d^64s^2$; body-centered-cubic (bcc) structure below 17 GPa and hexagonal-close-packed (hcp) structure above), Co (Z=26; $[Ar]3d^74s^2$; hcp structure below 100 GPa), Ni (Z=28; $[Ar]3d^84s^2$); face-centered-cubic (fcc) structure, Mo (*Z*=42; $[Kr]4d^55s$; bcc structure), Ag (Z=47; $[Kr]4d^{10}5s$; fcc structure), Pt (Z=78; $[Xe]5d^95s$; fcc structure) and Au (Z=79; $[Xe]5d^{10}5s$; fcc structure). State-of-the-art and homogeneous techniques for the experimental and theoretical EoS determinations have been used for all these metals.

On the experimental side, the EoS is measured by synchrotron x-ray diffraction in a diamond anvil cell (DAC). The accuracy of experimental EoS under high pressure has been improved in the last decade,[3,5,6] down to $\Delta V/V \simeq 0.5 \times 10^{-3}$ and $\Delta P \simeq \pm 3$ GPa at 150 GPa. The three main reasons for this improvement are the following: The use of helium as a pressure transmitting medium reduces nonhydrostatic stress on the sample.[7,8] Highly focused and intense x-ray beam[9] allows to diminish the sample size and as a consequence, to generate a more homogeneous pressure on it and on the adjacent small pressure gauge. The systematic uncertainty of the DAC pressure metrology, namely the ruby pressure gauge, has been much reduced.[3,10–14] The pressure scale calibration is statistically improved here by taking into account previous[3,15] and present metals' EoS.

On the theory side, density-functional theory[16,17] (DFT) provides the most used framework for these calculations, especially with the use of the local density approximation[18–20] (LDA)/generalized gradient approximation[21,22] (GGA). Among the numerous techniques used to solve the DFT problem, the projector augmented-wave method[23] (PAW) is one of the most powerful. Before its introduction, DFT techniques were divided into two classes: (i) the "all-electron" methods,[24] accurate (because the true density of the system can be accessed) and computationally expensive and (ii) "pseudopotential" approaches,[25] light, easy to implement but slightly inaccurate (due to the frozen-core approximation and the use of "pseudo" quantities instead of the true ones). PAW method has considerably improved the situation by unifying the two approaches in a unique formalism, preserving all advantages. It theoretically has the accuracy of "all-electron" methods and the efficiency of "pseudopotential" approaches.

TABLE I. Conditions of each experimental run.

Run	P range (GPa)	P Gauge	Samples	Diamond culet Size (μm)
1	0–36	Ruby	Ag+Fe+Mo+Ti	400
2	35–122	Ruby	Ag+Fe+Mo	100×300
3	17–46	Ruby	Ag+Fe	150×350
4	0–19	Ruby	Ni+Zn+Co	400
5	3–63	Ruby	Ni+Zn+Co	150×350
6	12–156	Ruby+He	Ni+Zn6+*c*-BN	100×300

We have generated our own PAW atomic data set for each metal, valid over a wide range of pressure. The accuracy of PAW vs all-electron techniques is discussed. However, the PAW method has the same limitation as all DFT approaches, which is the approximation potential for the exchange-correlation electronic interaction. Two widely used exchange-correlation functionals [LDA (Ref. 20) and GGA-PBE (Ref. 22)] and a new one [GGA-PBEsol (Ref. 26)] are tested here by the comparison with experiment. General trends for biases in the calculated *ab initio* EoS of transition metals are extracted.

II. EXPERIMENTAL METHODS

Six experiments have been performed with a similar sample geometry. Two to four samples have been loaded in a membrane diamond anvil cell with a large x-ray aperture, ensured by the use of a boron diamond support. All samples have been selected from commercial powders (purity from 98.8% to 99.9%) and chosen with a thickness smaller than 4 μm. Helium was the pressure transmitting medium. The pressure was estimated from the pressure calibration of the luminescence of a 3–4 μm ruby ball.[27] Experimental conditions of the six runs are summarized in Table I. The monochromatic x-ray signal diffracted by the samples has been collected on a MAR345 imaging plate system, located at a distance of $\simeq$400 mm from the sample, on the ID30 or ID27[9] beamlines of the European Synchrotron Radiation Facility. The diffraction geometry was determined using a silicon reference sample. The signal was circularly integrated using the FIT2D software[28] and *d*-spacings were individually determined. The samples were fine powders in the case of Co, Fe, Ag and a few single crystals in the case of Ni, Zn, and Mo.

III. PRESSURIZING CONDITIONS

It has been known for a long time that nonhydrostatic pressurizing conditions of the sample in a DAC lead to biased EoS measurements. In 1981, Bell *et al.* qualitatively showed that nonhydrostatic stress remained negligible up to 60 GPa in a helium sample compressed in a DAC.[29] Since then, helium has had the reputation of being the best pressure transmitting medium, which creates a hydrostatic (or nearly hydrostatic) stress around the sample. Quantitative measurements confirmed that the nonhydrostatic stress remains negligible up to at least 50 GPa in metallic samples compressed in helium.[7] From these studies, we can infer that pressurizing conditions were nearly hydrostatic during runs 1, 3, 4 and 5 because they were performed in a moderate pressure range (see Table I) and because the thin samples remained embedded in helium (no bridging between diamond anvils). The pressurizing conditions (in particular, the macroscopic nonhydrostatic stress) for run 2, the high-pressure run for Ag and Mo, have been characterized in Ref. 8, on the basis of x-ray diffraction lines shifts. The nonhydrostatic stress was negligible up to 98 GPa, but increased dramatically above that pressure because of the bridging of the samples between the diamond anvils. For this reason, the P-V points measured above 100 GPa during run 2 will not be taken into account in the EoS analysis presented below. For run 6, the single-crystal x-ray diffracted spots recorded for nickel correspond to the same lattice parameter within $\delta a/a = \pm 1.5 \times 10^{-4}$, a scatter that can be attributed to instrumental factors (for instance, the uncertainty in the position of the center of the imaging plate). There was thus no evidence for x-ray diffraction lines shift caused by nonhydrostatic compression up to the highest pressure reached in this run. To sum up, the data presented here are free from any bias due to nonhydrostatic compression, if the points from run 2 above 100 GPa are excluded.

IV. COMPARISON BETWEEN EXPERIMENTAL EQUATIONS OF STATE; IMPLICATIONS FOR PRESSURE CALIBRATION

The measured P-V data points are presented in Tables II and III and plotted in Fig. 1. The pressures given by two calibrations of the ruby gauge are reported in Tables II and III: P_R for Mao *et al.* calibration[27] and P'_R for Dewaele *et al.* calibration.[3] For silver and molybdenum, the atomic volumes measured up to 100 GPa only are reported because the compression became nonhydrostatic above that pressure.[8]

For each metal, the $P(V)$ data have been fitted with a Vinet EoS formulation.[30] This EoS expresses as

$$P = 3K_0\left(\frac{V}{V_0}\right)^{-2/3}\left[1-\left(\frac{V}{V_0}\right)^{1/3}\right]\exp\left\{\frac{3}{2}(K'_0-1)\times\left[1-\left(\frac{V}{V_0}\right)^{1/3}\right]\right\}. \quad (1)$$

The three parameters of a Vinet EoS are thus the volume V_0, the isothermal bulk modulus K_0 and its pressure derivative K'_0 at ambient pressure. The parameters K_0 and K'_0 obtained by fitting this EoS to the present data (using Dewaele *et al.*[3] pressure scale, P'_R) are presented in Table IV. For all studied metals, V_0 has been deduced from the low-pressure measurements ($0 \leq P \leq 5$ GPa); the value of V_0 was then fixed during the whole data set fitting. The fitting results for ϵ-iron are presented elsewhere[15] and are not discussed here. For the other metals, the fitted K_0 and K'_0 are presented in the third column of Table IV.

Ultrasonic (US) isothermals K_0 are also reported in Table IV, fifth row, and those are compared to DAC K_0 in Fig. 2(a). The large range of literature values for ultrasonic K_0 of zinc

TABLE II. Atomic volumes of Ag, Mo and Ni, Zn, Co, measured by angle dispersive x-ray diffraction, with helium pressure transmitting medium, as a function of the ruby luminescence pressure. P_R is the pressure obtained from the "classical" calibration (Ref. 27), and P'_R from the calibration from Ref. 3. In run 6, helium pressure transmitting medium has been used as an alternative pressure gauge above 65 GPa. Its EoS has been taken from Ref. 73: It can be described by the Vinet formulation, with the following parameters $V_0=24.804$ Å^3/at, $K_0=0.165$ GPa, $K'_0=7.483$. The numbers between parentheses indicate pressure from helium EoS. Experimental uncertainty on V is 0.01 Å^3/at. Uncertainty on P_R increases from 0.05 GPa at 1 GPa to 2 GPa at 150 GPa, if the ruby pressure scale is assumed to be correct.

P_R (GPa)	P'_R (GPa)	Ag V(Å^3/at)	Mo V(Å^3/at)	P_R (GPa)	P'_R (GPa)	Ni V(Å^3/at)	Zn V(Å^3/at)	Zn a(Å)	Zn c(Å)	Co V(Å^3/at)	Co a(Å)	Co c(Å)
			Run 1						Run 4			
1.8	1.8	16.7256	15.4547	0	0	10.9423	15.2125	2.6644	4.9487	11.0966	2.5071	4.077
5.2	5.21		15.2764	1.5	1.5	10.8504	14.8719	2.6573	4.8639	11.0018	2.5	4.0652
8	8.03	15.9444	15.1336	2.6	2.6	10.7841	14.6605	2.6515	4.8156	10.9294	2.4945	4.0562
8.6	8.64	15.8905	15.1013	5.1	5.1	10.6565	14.1771	2.6409	4.6946	10.807	2.4854	4.0402
10	10	15.7542	15.0365	7.8	7.8	10.5302	13.7923	2.6308	4.6021	10.6738	2.4751	4.0237
12.2	12.3	15.5552	14.9217	8.8	8.8	10.4821	13.6458	2.627	4.5664	10.6285	2.4716	4.0179
14.5	14.6	15.3331	14.8127	11.4	11.5	10.3638	13.3401	2.6174	4.4971	10.5131	2.4629	4.0025
17.5	17.7	15.1011	14.6816	13.0	13.1	10.2789	13.1352	2.6099	4.4533	10.4374	2.4574	3.9916
19.7	19.9	14.9195	14.5842	15.2	15.3	10.1833	12.9185	2.6013	4.4089	10.3476	2.4507	3.9788
21.2	21.4	14.8156	14.5232	18.3	18.5	10.0737	12.6593	2.5896	4.3597	10.2132	2.439	3.9649
23.8	24.1	14.6409	14.4158					Run 5				
26.9	27.3	14.4428	14.2865	3.5	3.5		14.4649	2.6483	4.763	10.8918	2.491	4.0538
30	30.4	14.271	14.1817	6.7	6.7	10.5796	13.9492	2.6359	4.6365	10.7286	2.4787	4.0327
35.5	36.1	13.9785	13.9833	10.2	10.2	10.4114	13.4697	2.6216	4.5261	10.5433	2.4657	4.0048
33.1	33.6	14.1171	14.059	13.6	13.7	10.2672	13.1401	2.6107	4.4523	10.4193	2.4548	3.993
0	0	17.0212	15.5584	16.3	16.4	10.1525	12.8421	2.5977	4.395	10.3115	2.4463	3.9793
		Run 2		20.3	20.5	9.9995	12.4976	2.581	4.3326	10.1537	2.4333	3.9604
35.5	36.1	13.9244	13.9507	26.4	26.7	9.7994	12.0501	2.5597	4.2473	9.93259	2.417	3.9266
46.1	47.1	13.4615	13.5649	30.7	31.1	9.6564	11.8052	2.5459	4.2062	9.79297	2.4063	3.9058
54.3	55.6	13.1249	13.3184	35.5	36.1	9.5116	11.5185	2.529	4.1591	9.65309	2.3936	3.8909
62.4	64.2	12.8244	13.0825	40.6	41.3	9.3531	11.2621	2.5124	4.1204	9.50567	2.3817	3.8699
68.1	70.2	12.6301	12.9196	45.5	46.5	9.2232	11.031	2.4967	4.0868	9.36221	2.3694	3.8513
73.2	75.6	12.4705	12.7749	50.2	51.4	9.1077	10.8351	2.4834	4.0573	9.24947	2.3597	3.8363
78.4	81.2	12.3348	12.6526	54.8	56.2	8.9910	10.64	2.4696	4.0289	9.11345	2.3499	3.8115
84.3	87.5	12.188	12.5133	58.5	60.1	8.9092	10.5198	2.4614	4.01	9.0531	2.3421	3.8114
88.8	92.3	12.0738	12.4096	63.4	65.2	8.8067	10.3593	2.4502	3.985	8.92911	2.3317	3.7928
94	97.9	11.9548	12.2937					Run 6				
100	104	11.803	12.1408	12.8	12.9	10.289	13.1408	2.6088	4.4589			
108	113	11.6461	11.9969	24.7	25.0	9.8373	12.1386	2.5637	4.2652			
116	122	11.5135	11.8289	37.5	38.1	9.4545	11.4242	2.5198	4.1552			
		Run 3		49.0	51.0	9.104	10.814	2.4813	4.0561			
17.6	17.8	15.0723		(63.2)	(65)	8.8219	10.355	2.449	3.9871			
22.6	22.9	14.7065		(72.7)	(75.1)	8.6623	10.099	2.4299	3.9499			
29.8	30.3	14.268		(81.3)	(84.2)	8.5267	9.8573	2.4104	3.9181			
37.4	38	13.8647		(89.0)	(92.5)	8.3894	9.7164	2.3977	3.9031			
42.1	42.9	13.6326		(94.1)	(98.1)	8.3124	9.5624	2.3877	3.8737			
46.2	47.2	13.4703		101.2	106	8.1966	9.4104	2.3747	3.8536			
				(109.7)	(114.9)	8.0621	9.2178	2.3612	3.8183			
				(110)	(115.3)	8.0644	9.2116	2.361	3.8163			
				(114)	(119.6)	8.0134	9.1208	2.3529	3.8047			
				(121.8)	(128.2)	7.9236	8.9973	2.3425	3.7866			
				(127.5)	(134.5)	7.855	8.8927	2.334	3.7698			
				(134.5)	(142.2)	7.7731	8.7828	2.3245	3.7537			
				(140.4)	(148.8)	7.7132	8.6844	2.3166	3.7371			
				(147.4)	(156.6)	7.6279	8.5792	2.3085	3.7177			

TABLE III. Atomic volume of Fe $V_{bcc/hcp}$ as a function of the ruby luminescence P_R [Mao *et al.* scale (Ref. 27)] or P'_R [Dewaele *et al.* scale (Ref. 3)], or tungsten pressure P_W (EoS from Ref. 3, see Ref. 15). The last column (a_W) gives the lattice parameter of tungsten measured during the run #5 described in Ref. 15.

P_R (GPa)	P'_R (Å)	$V_{bcc/hcp}$ (Å^3/at)	c/a hcp	P_W (GPa)	V_{hcp} (Å^3/at)	c/a hcp	a_W (Å)
		Run 1				Run #5 from Ref. 15	
1.8	1.8	11.634		28.1	9.8802	1.602	3.0833
5.2	5.2	11.428		55.2	9.1604	1.5987	3.0241
8	8.0	11.256		78.4	8.74	1.5975	2.9824
8.6	8.6	11.233		105	8.3254	1.5954	2.9408
10	10.0	11.152		122	8.1093	1.5968	2.9182
12.2	12.3	11.045		136	7.9487	1.5979	2.9004
14.5	14.6	10.935		146	7.8436	1.5973	2.8882
17.6	17.7	10.296	1.6045	157	7.7307	1.5974	2.875
19.7	19.9	10.201	1.6028	167	7.6604	1.597	2.865
21.2	21.4	10.148	1.6039	176	7.5693	1.6012	2.8554
23.8	24.1	10.042	1.6014	188	7.4474	1.5973	2.8422
27.0	27.3	9.936	1.6023	197	7.3906	1.5964	2.8339
30	30.4	9.841	1.6011				
35.5	36.1	9.674	1.6016				
33.1	33.6	9.742	1.6013				
4.0	4.01	11.522					
1.3	1.3	11.676					
0	0	11.754					
		Run 3					
17.7	17.8	10.282	1.6036				
22.6	22.9	10.086	1.6024				
29.9	30.3	9.8338	1.6011				
37.4	38	9.593	1.6008				
42.1	42.9	9.464	1.6003				
46.2	47.2	9.356	1.5997				
		Run 2					
35.5	36.1	9.652	1.6007				
46.1	47.1	9.366	1.5976				
54.3	55.6	9.155	1.5997				
62.4	64.2	8.963	1.6013				
68.1	70.2	8.854	1.5989				
73.2	75.6	8.752	1.5996				
78.4	81.2	8.659	1.5997				
84.3	87.5	8.553	1.5989				
94.0	97.9	8.401	1.5995				

is due to the large elastic anisotropy of this metal. The lower limit of K_0 corresponds to a Reuss averaging of its single-crystal elastic constants, while the upper limit corresponds to a Voigt averaging. The pressure distribution in a DAC pressure chamber is expected to be close to isostress; we thus chose a value close to Reuss K_0 as the reference ultrasonic value. It is found that when the P'_R pressure scale is used, ultrasonic and DAC K_0 agree within $\pm 3.5\%$ for the metals studied in this work, the metals studied in our recent work[3] and for diamond.[31] Recently, the ultrasonic and DAC K_0 of *c*-BN have also been reconciled by the use of the P'_R scale.[32] The ultrasonic vs DAC agreement is closer with the current DAC data than with literature DAC compression data for silver,[33] molybdenum[34] and cobalt.[35] We explain the improvement by the use of better pressurizing conditions and/or a better calibrated pressure gauge. In fact, the DAC EoS of silver was measured using a gold x-ray pressure gauge,[33] with a calibration that underestimates the pressure:[3] the resulting K_0 was underestimated. Similarly, the bulk modulus of cobalt[35] was overestimated because of the pressure overestimation by the platinum pressure gauge calibration.[3,36] The DAC EoS of Mo has been measured by radial diffraction

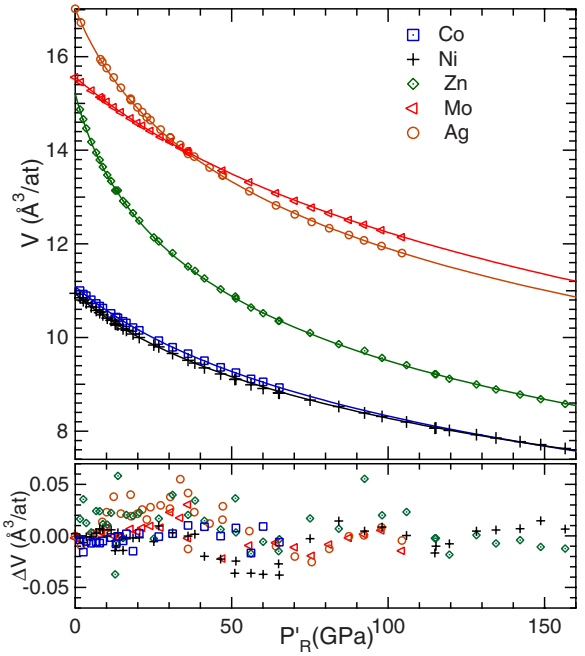

FIG. 1. (Color online) Measured atomic volumes of Co, Ni, Zn, Mo, and Ag as a function of pressure using a recently updated pressure scale (Ref. 3) (pressure gauges: see Tables I and II). The continuous lines are the fitted EoS (see Table IV, third column). The difference between the data points and the fitted EoS is presented in the lower part of the figure.

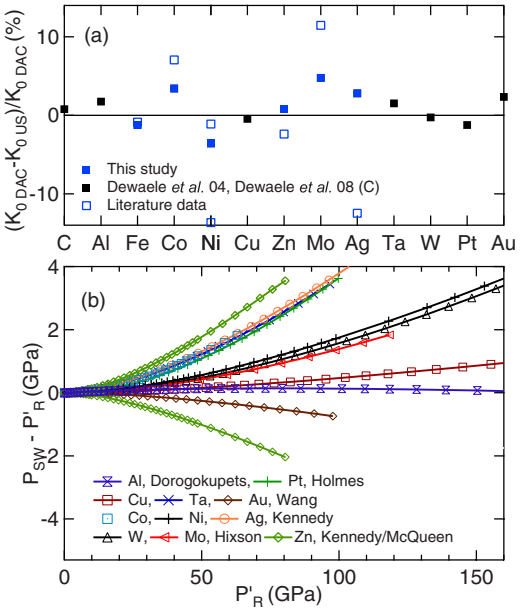

FIG. 2. (Color online) (a) Relative difference between the bulk moduli measured by US experiments and compression in a DAC. These moduli are given in Table IV, third and fifth columns, in Ref. 3 (Table II) and Ref. 6. (b) Difference between reduced shock-wave pressure P_{SW} and static pressure P'_R for a given atomic volume of eleven different metals. P_{SW} and P'_R are calculated using Vinet EoS and the parameters from Table IV (Co, Ni, Ag, Mo, Zn) or reported in Ref. 3 (Al, Pt, Cu, Ta, W) and Ref. 8 (Au).

under nonhydrostatic compression;[34] this method, aimed at measuring the yield stress of materials under high pressure, does not lead to accurate EoS parameters. Apart from the early work by Vaidya and Kennedy[37] in which a pressure of 4.5 GPa only was reached, we are not aware of any static compression EoS data for nickel. The EoS of α-Fe, measured below 15 GPa by Mao *et al.*[38] using NaCl as an x-ray pressure gauge, is in very good agreement with the current EoS. The DAC EoS of zinc has been measured up to 123 GPa using helium pressure medium by Takemura;[39,40] its bulk modulus is close to ours, the difference being due to the ruby pressure scale used (P_R scale for Takemura, P'_R scale for this study). To sum up, the good agreement between ultrasonic and DAC bulk moduli obtained in the current study validates the calibration of the ruby gauge used in the current study. The bulk modulus is constrained mostly by the beginning of the compression curve (up to $V/V_0 \simeq 0.9$); this validation holds for moderate pressures. At high compression, the lack of ultrasonic K'_0 measurements (see Table IV) renders the reduced shock-wave (RSW) EoS the most useful data set for

TABLE IV. Parameters of the Vinet EoS (Ref. 30) obtained by least-squares fit of the experimental compression data in DAC for α-Fe, Co, Ni, Zn, Mo, and Ag. The parameters of these EoS are V_0, volume, K_0, bulk modulus and K'_0, its pressure derivative, under ambient conditions. The bold values have been fixed during the fitting procedure. Numbers between parentheses are published error bars or fitting error bars (95% confidence interval) on the last or the two last digits. K_0 and K'_0 measured by ultrasonic (US) and shock-wave (SW) compression experiments (fit by a Vinet EoS) are also reported for comparison. US K'_0 have not been measured for Co, Ni, and Zn.

Metal	V_0 (Å^3)	K_0(GPa), K'_0 DAC, P'_R	K_0(GPa), K'_0 DAC, P'_R	K_0(GPa), K'_0 US	Ref. US	K_0(GPa), K'_0 SW	Ref. SW
α-Fe	**11.760**	171(11),4.34(2.10)	**165**,5.47(51)	165,5.29	74		
Co	**11.096**	190.5(2.9),4.38(18)	**184**,4.73(6)	184(5),?	75	**184**,4.93(4)	42
			190,4.37(4)			**190**,4.67(3)	42
Ni	**10.942**	176.7(2.5),5.23(9)	**183**,4.99(2)	183(3),?	76	**183**,5.13(1)	42
Zn	**15.213**	60.5(9),5.69(7)	**60**,5.73(1)	59(3)–72(3),?	77	**60**,5.6–5.95	45,42
Mo	**15.558**	274.1(3.2),3.58(12)	**261**,4.06(5)	261(3),4.46	78	**261**,4.18(2)	43
Ag	**17.021**	103.9(1.4),5.78(9)	**101**,5.97(2)	101(2),6.15	79	**101**,6.19(1)	42

a comparison with DAC EoS. The RSW EoS of each metal has an uncertainty (relative error bars between 3 and 10% are reported), as will be shortly discussed below.

In dynamic compression experiments, shock and particle velocities are measured during the shock. Then, the pressure, the volume and the internal energy are calculated using the Rankine-Hugoniot relations.[41] The *P-V* shock data can then be reduced to ambient temperature, in most cases using a Mie-Grüneisen quasi-harmonic formalism.[42,43] The following RSW EoS have been used here: Ref. 42 for Co, Ni, and Ag; Ref. 43 for Mo; Ref. 14 for Al; Ref. 42 and Refs. 44–46 for Zn. The various published RSW EoS can be discrepant for a given element, for instance in the case of aluminum and zinc. As a matter of fact, the disagreement between Refs. 13 and 3 calibrations of the ruby pressure gauge is due to a different choice of the RSW EoS of aluminum. DAC EoS used in these two studies are identical, and the corrections for finite yield strength in shock-wave measurements performed by Chijioke *et al.*[13] were small in the range of interest (0.7 GPa in average at 150 GPa). The aluminum RSW EoS used by Refs. 3 and 13 have been taken respectively from Refs. 47 and 48. They differ by 12 GPa at 150 GPa (RSW EoS being stiffer in Ref. 48). In this work, we have thus considered an alternative RSW EoS which has been calculated in Ref. 14 and is based on an independent shock-wave database. It has the following Vinet parameters: K_0 =73.46 GPa, K_0'=4.52. It can be considered as a compromise between the two extreme curves previously used (it differs from Ref. 47 RSW EoS by 2 GPa at 150 GPa). In the case of zinc, the published RSW EoS are not in mutual agreement.[42,44–46] This can be due to the scattering of the shock and particle velocity measurements or to errors in the reduction procedure. RSW EoS of Zn is particularly sensitive to reduction, because of the high temperature reached along the Hugoniot for this metal: ≃3100 K at 100 GPa. The melting of zinc occurs around 80 GPa along the Hugoniot. We have thus fitted the various RSW EoS[42,44–46] below the estimated melting pressure, which led to K_0' values that vary between 5.60 (Ref. 45) to 5.95 (Ref. 42) (see Table IV).

The values of K_0' obtained by fitting DAC and RSW EoS data by a Vinet equation, K_0 being fixed to its ultrasonic value, are presented in Table IV. The fits were performed in the *P* range of the current DAC measurements. For most of the metals studied here, the RSW K_0' is slightly higher than the DAC K_0'. In other words, the pressure given by RSW EoS becomes higher than P_R' (Ref. 3) at very high pressure. The difference between these two pressures is plotted in Fig. 2(b), for the metals studied here and in our previous report.[3] The current data set is the most extended basis for a refinement of the calibration of the ruby gauge calibration using RSW EoS. It includes now 11 metals, whose DAC EoS have been measured using identical techniques and with the same accuracy. Possible errors in RSW EoS are expected to be statistically reduced when the average of many RSW EoS is considered, if they have no systematic bias and if they are mutually independent. For the correct ruby scale calibration, the difference between the static EoS and the RSW EoS should be zero when averaged over the 11 metals.

Figure 2(b) suggests that the pressure calibration P_R' underestimates the pressure by approximately 2.5 GPa at 160 GPa. We have not taken into account the RSW EoS of zinc because of its large uncertainty. A new calibration of the ruby gauge can be obtained by minimizing $P_{SW}-P_R'$ in average for the ten remaining metals. If the ruby pressure formula proposed by Mao *et al.*[27] is assumed to be correct [$P=A/B[(\lambda/\lambda_0)^B-1]$, λ being the ruby luminescence wavelength], the parameters which allow to minimize these ten RSW EoS pressures and ruby pressure are $A=1920$ GPa and $B=9.61$. The pressure given by various ruby gauge calibrations,[3,10,11,13,14] with reference to the Mao86 calibration,[27] is presented in Fig. 3, together with the present calibration. It can be shown that the present upgrade confirms closely the proposals from Refs. 10, 11, 13, and 14. The agreement with Dorogokupets and Oganov calibration[14] seems nearly perfect. The form proposed in Ref. 13 deviates from our upgrade for the highest pressures reached in the current study.

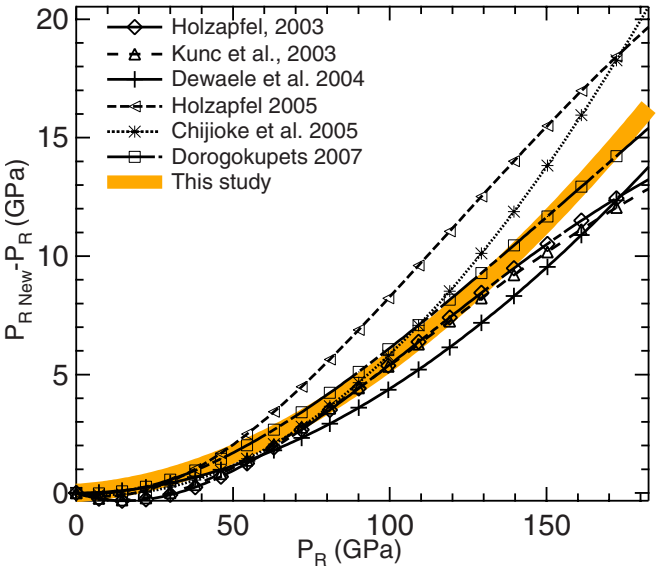

FIG. 3. (Color online) Difference between recently proposed ruby calibrations (Refs. 3, 10, 11, 13, and 14) and Mao *et al.* calibration (Ref. 27). The solid orange (gray) curve corresponds to a fit of the average of pressures calculated using the RSW EoS of ten metals compressed with a ruby gauge (see Fig. 2). The equation proposed by Mao *et al.* (Ref. 27) has been used for this fit: $P=A/B[(\lambda/\lambda_0)^B-1]$. The parameters $A=1920$ GPa and $B=9.61$ have been obtained.

V. COMPUTATIONAL DETAILS

This section is devoted to the computation of equations of state employing one of the most successful techniques in the framework of the Kohn-Sham density-functional theory, namely the PAW method.[23] The aim of this work is to test the validity of PAW formalism from equilibrium state to high pressure conditions, using PAW atomic data sets suitable for a wide range of pressure.

A. PAW method

The framework of this study is the DFT, using LDA or GGA approximation, applied in the frame of the PAW

method. We will not go into technical details about PAW here as several papers already proposed a description of its formalism and practical implementation.[23,49–52] However, for a better understanding of the following sections, it is useful to emphasize the key concepts of the method. Only valence electrons are explicitly treated during the calculation; core electrons are frozen around the nucleus. The PAW method is based on the coupling of two basis to develop the electronic wave functions: (i) a plane-wave basis on which "pseudo" (smooth) quantities are expressed and (ii) a local basis (partial-wave basis), centered around nuclei, used to retrieve "true" quantities from "pseudo" ones. Computation is light as smooth wave functions are computed and accurate as exact wave functions can always be retrieved. The local basis is defined in nonoverlapping spheres delimited by a radius r_{PAW} controlling the smoothness of pseudo wave functions. As the pseudo quantities are built without any "norm-conserving" constraint (*ultrasoft* scheme), the use of a compensation charge density is necessary to retrieve the right norm of the density. This compensation charge density is analytically expressed and localized around nuclei inside spheres of radius r_{comp}.

Thus, the accuracy of the PAW method is influenced by three monitorable parameters: (i) the number of frozen-core electrons, (ii) the size of the plane-wave basis, and (iii) the size of the partial-wave basis. Frozen-core approximation can be tested by the inclusion of more electrons in the valence band (this is done in the present study by the systematic use of two PAW data sets for each metal; see Sec. V B). The size of the plane-wave basis is controlled by a cut-off kinetic energy; the size of the partial-wave basis can be increased by the inclusion of more partial waves per atom; for our study, we have checked that the use of additional partial waves had no influence on the computed EoS.

It has been demonstrated that even for the heaviest metals studied here (platinum and gold), the influence of spin-orbit coupling on the calculated energy and EoS of the system is negligible.[53] Spin-orbit coupling has thus been neglected here.

Within the LDA/GGA approximation, the calculated values will be influenced by the choice of an exchange-correlation functional. As a consequence, the validity of PAW results should always be done in comparison with results obtained by all-electron methods which use the same functional. For this reason, we compare all our results with points obtained by full-potential linearized augmented-plane-wave[54] (FP-LAPW) approach (when available). We have investigated one LDA—Perdew-Wang 92[20] (PW92)—and two GGA functionals: Perdew-Burke-Ernzhofer 96[22] (PBE) and the newly proposed PBEsol[26] functional. As PBEsol aims at better describing the bulk properties of materials, it is important to test its performance to predict high-pressure EoS.

B. PAW data sets

Every PAW calculation needs several quantities defining the atomic species and the partial-wave basis for each type of atom. Such a set of parameters is called "PAW data set." As emphasized in Sec. V A, key parameters of such a data set are the following: (i) the number of electrons treated in the valence, (ii) the exchange-correlation functional (LDA, GGA-PBE or GGA-PBEsol), (iii) the r_{PAW} and r_{comp} radii (while a small overlap can be admitted for PAW spheres, it is not recommended to permit overlap of compensation charge densities), and (iv) the number of partial waves (and associated projectors).

In the present study, as we aim at compressing the metals and thus have PAW atomic data valid for a large range of pressure/volumes, we have generated our own PAW data sets. We have tested the validity of the frozen-core approximation by using two data sets per metal (with inclusion or not of *semicore* states). We have chosen small enough radii r_{PAW} and r_{comp}. We have included two partial waves per angular momentum in the local basis, except for Zn (with *semicore* states) for which $3p$ partial waves were necessary to have accurate enough pressures.

The code used for the generation of PAW data sets is ATOMPAW.[55,56] A special attention to the efficiency of pseudization schemes (in terms of softness) has been taken. All PAW data set parameters for Fe, Co, Ni, Zn, Mo, Ag, Pt, and Au are listed in Table V.

C. DFT calculations

To perform PAW-DFT calculations we used the ABINIT[51,57–59] code. For each metal, pressure has been deduced from the computed stress tensor for a given set of volumes. In the case of ϵ-Fe, Zn and Co, the hexagonal parameter c/a has been optimized for each volume, as forces and stresses are straightforwardly expressed in PAW. This capability of relaxing structure and/or unit cell is clearly an advantage of PAW over all-electron techniques.

As we are interested in the computation of pressures, all convergence parameters have to be adjusted in order to get a target accuracy on pressure. In the present study, size of plane-wave basis and Brillouin zone sampling have been chosen in order to get pressure with a precision better than 0.1 GPa. We also checked that, for these parameters, c/a cell parameter and magnetic moment were converged. Table V exhibits chosen parameters for each metal.

Finally note that the use of a smearing scheme[60] (with $\sigma=0.2$ eV) was necessary to reduce the number of k-points needed to reach convergence.

VI. COMPARISON BETWEEN CALCULATED AND EXPERIMENTAL EQUATIONS OF STATE

DFT-PAW EoS and their parameters, obtained by a Vinet fit[30] in the same pressure range as experimental data, are plotted in Fig. 4 and presented in Table VI. For each metal, we compare our calculations with our experimental points and fits. To perform this comparison, thermal pressure has been estimated using the Debye form presented in Ref. 15, which includes zero-point motion. $P_{\mathrm{TH}}(V,298\ \mathrm{K})$ value is weakly dependent on compression and has been considered constant in the pressure range studied here. The Debye parameters for all studied metals have been taken from the

TABLE V. Contents of PAW data sets for metals and parameters for DFT used in the present work for EoS computation. For each metal two PAW sets have been used: one data set without explicit treatment of semicore states (*without semicore*) and the other with inclusion of semicore states in the valence (*with semicore*). "Valence orbitals" indicate which orbitals are treated as valence orbitals in the PAW calculation and the electronic configuration chosen to solve atomic problem during PAW data set generation. r_{PAW} is the radius of PAW spheres and r_{comp} is the radius used to define the compensation charge density. All PAW data sets contain two *s*, two *p* and two *d* partial waves, except Zn with semicore for which the addition of a third *p* partial wave was necessary. "Plane wave cutoff" and "*k*-pts in BZ" are the values of the cutoff energy of plane-wave basis and the number of *k*-points in the whole Brillouin zone needed to compute the pressure with a precision of 0.1 GPa.

Metal		Valence orbitals	r_{PAW} (a.u.)	r_{comp} (a.u.)	Plane wave cutoff (eV)	*k*-pts in BZ	Structure[a]
α-Fe	Without semicore	$3d^7 4s^1$	2.3	2.0	410	20^3	bcc FM
	With semicore	$3s^2 3p^6 3d^7 4s^1$	2.0	2.0	545	20^3	bcc FM
ϵ-Fe	Without semicore	$3d^7 4s^1$	2.3	2.0	410	14^3	hcp AF type II
	With semicore	$3s^2 3p^6 3d^7 4s^1$	2.0	2.0	545	14^3	hcp AF type II
Co	Without semicore	$3d^8 4s^1$	2.3	2.0	410	16^3	hcp FM
	With semicore	$3s^2 3p^6 3d^8 4s^1$	2.1	2.1	680	14^3	hcp FM
Ni	Without semicore	$3d^9 4s^1$	2.3	2.0	410	14^3	fcc FM
	With semicore	$3s^2 3p^6 3d^9 4s^1$	2.1	1.6	680	14^3	fcc FM
Zn	Without semicore	$3d^{10} 4s^2$	2.3	1.8	410	16^3	hcp NM
	With semicore	$3s^2 3p^6 3d^{10} 4s^2$	2.0	1.6	680	16^3	hcp NM
Mo	Without semicore	$4d^5 5s^1$	2.8	2.0	410	18^3	bcc NM
	With semicore	$4s^2 4p^6 4d^5 5s^1$	2.2	2.2	680	18^3	bcc NM
Ag	Without semicore	$4d^{10} 5s^1$	2.4	2.0	410	18^3	fcc NM
	With semicore	$4s^2 4p^6 4d^{10} 5s^1$	2.0	2.0	545	18^3	fcc NM
Pt	Without semicore	$5d^9 6s^1$	2.5	2.25	545	18^3	fcc NM
	With semicore	$4f^{14} 5p^6 5s^2 5d^9 6s^1$	2.3	2.25	680	18^3	fcc NM
Au	Without semicore	$5d^{10} 6s^1$	2.5	2.25	545	18^3	fcc NM
	With semicore	$4f^{14} 5p^6 5s^2 5d^{10} 6s^1$	2.3	2.25	680	18^3	fcc NM

[a]NM: nonmagnetic, FM: ferromagnetic, AF: antiferromagnetic.

literature,[15,61–65] which led us to the following estimates of $P_{TH}(V, 298\ \text{K})$: 1.0 GPa for Fe, 1.5 GPa for Co, 2.0 GPa for Ni, 1.4 GPa for Zn, 1.6 GPa for Mo, 1.1 GPa for Ag, 1.5 GPa for Pt, and 1.4 GPa for Au. All-electron FP-LAPW results are also plotted in Fig. 4, when available, as references for DFT.

A. Quality of PAW results

Each graph presented in Fig. 4 exhibits six PAW equations of state, using LDA, GGA-PBE or GGA-PBEsol exchange-correlation functional, including or not semicore states in the valence orbitals. LDA and GGA curves can clearly be differentiated. As usual, the equilibrium volumes V_0 predicted with GGA are higher than those predicted with LDA and the compression curves predicted with the three functionals are roughly parallel.

PAW EoS including semicore states reproduce available all-electron ones. The agreement is perfect at equilibrium volume and remains good for the whole range of pressure, either in LDA or GGA-PBE (when FP-LAPW points have been published). This demonstrates the high quality of our PAW data sets in a large range of compression. This was expected, since complete enough partial-wave basis and small enough values of PAW radii were used.

Except for cobalt—and iron within the frame of LDA—EoS are not influenced by the inclusion of semicore states. This means that frozen-core approximation is valid without the inclusion of semicore states in the considered range of pressure.

In addition to the equations of state, a perfect agreement is found between PAW and FP-LAPW for internal parameters: for hcp metals c/a ratios are identical (1.61 for Co at 0 GPa, 1.85 for Zn at 0 GPa, 1.61 for ϵ-Fe at 15 GPa);[46,66] for magnetic phases, the local magnetic moment is found to be in good agreement with FP-LAPW ($2.22\mu_B$ for FM α-Fe at 0 GPa, $1.52\mu_B$ for FM Co at 0 GPa, $0.58\mu_B$ for FM Ni at 0 GPa, $1.32\mu_B$ for AF ϵ-Fe at 15 GPa).[50,66] For iron and cobalt, the variation of the magnetic moment with respect to volume is found to be similar to the one of Ref. 66.

B. Comparison between experiments and calculations

The values of theoretical V_0 (equilibrium volume) and K_0 (bulk modulus at ambient pressure) obtained in LDA, GGA-PBE and GGA-PBEsol are plotted in Fig. 5, with reference

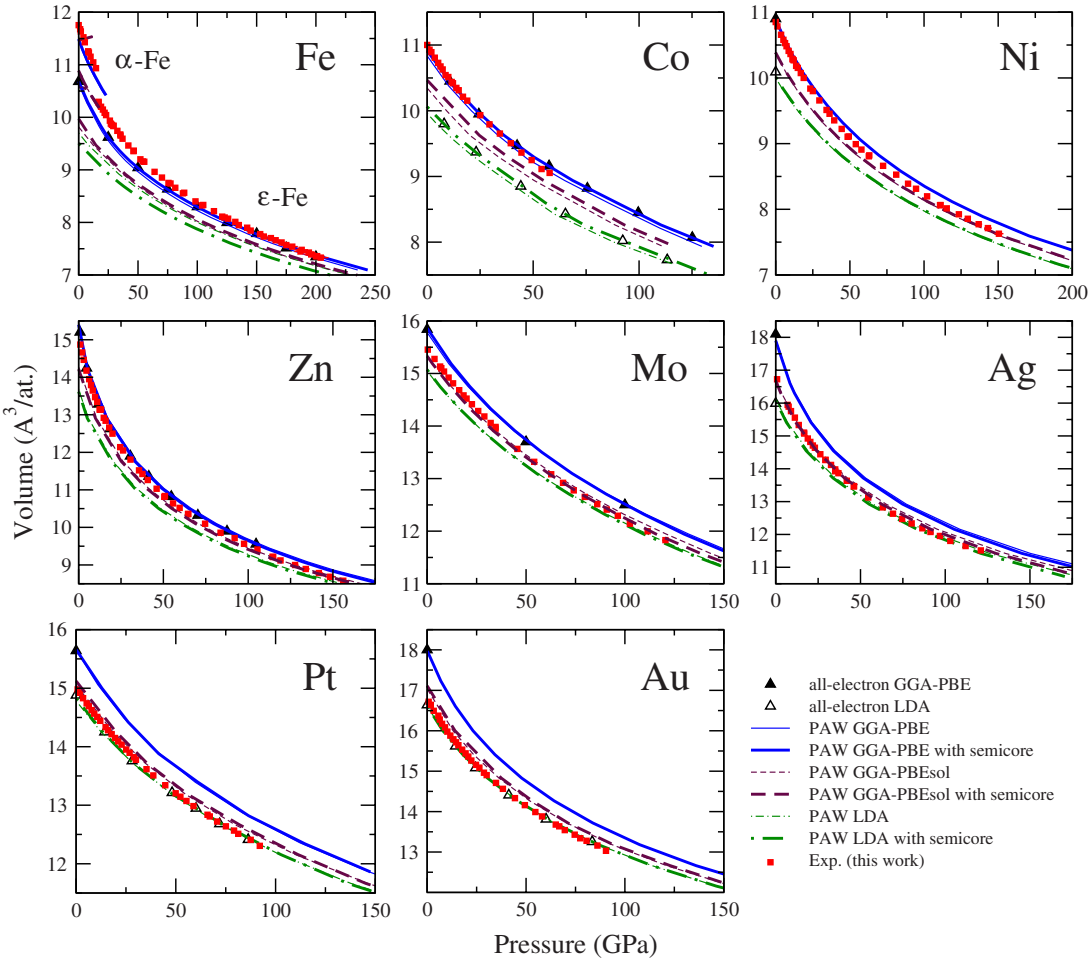

FIG. 4. (Color online) Theoretical and experimental static EoS of Fe, Co, Ni, Zn, Mo, Ag, Pt, and Au. Comparison between calculated and experimental data. The filled squares are experimental values taken from Tables II and III from which thermal pressure has been subtracted. Error bars on pressure, due to the uncertainty on pressure calibration, have been represented but they are in general smaller than the symbols size. The dashed-dotted lines (resp. solid lines, dashed lines) are PAW equations of states using LDA (resp. GGA-PBE, GGA-PBEsol) exchange-correlation functional. The thin curves (resp. bold curves) are PAW EoS obtained without inclusion (resp. with inclusion) of semicore states (see Table V). When only one curve is visible, both are superimposed. The empty (resp. filled) triangles are results of all-electron calculations published in literature using LDA (resp. GGA) exchange-correlation functional (FP-LAPW results for Fe[66], Co[66], Ni[50], Zn[46], Mo[70], Ag[71], Pt[71], Au[71]; FP-LMTO results for Pt[69], Au[69]). They have to be considered as references for PAW calculations.

to experimental V_0 and K_0. When V_0 is underestimated (in particular, by LDA calculations), K_0 is overestimated, which is due to the hardening of the lattice as it is compressed. This effect causes a linear trend that can be easily observed in Fig. 5, where the *ab initio* bulk modulus, normalized to the experimental one, is plotted as a function of the *ab initio* equilibrium volume, normalized to the experimental one. In fact, the slope of this trend is expected to be $\simeq -K_0'$, which has a similar value for all studied metals (see Table VI). We observe, as several authors before us,[67,68] that the effect of the gradient correction is to increase V_0 and decrease K_0 with respect to LDA values.

GGA-PBEsol gives EoS closer to experimental ones than GGA-PBE for 4*d* and 5*d* metals. However, GGA-PBE V_0 and K_0 are the most accurate in average over metals studied here, being respectively within $\pm 7\%$ and $\pm 20\%$ of experimental ones. In the following we will thus focus on GGA-PBE results.

The ratio between GGA-PBE and experimental ambient pressure bulk moduli for the metals studied here and in Ref. 3 is represented in Fig. 6. For a given row of the periodic table of elements, the GGA-PBE K_0 decreases, relatively to the experimental one, as the atomic number increases. It also decreases when the atomic number increases for metals with a similar valence electronic structure (as in the case of noble metals: the bulk modulus of gold is underestimated by 17%, while the bulk modulus of copper is accurate within 2%[3]).

The accuracy of GGA-PBE calculations under very high pressure (or compression) can be illustrated by the comparison between the values of experimental and theoretical K_0' (see inset of Fig. 5). GGA-PBE K_0' are all overestimated, except for α-Fe. There is no trade-off between GGA-PBE V_0 and K_0'. Bulk moduli of all studied metals will thus become overestimated at sufficiently high pressure. This can also be seen in Fig. 4: The GGA-PBE compression curves are too stiff. This effect is clearly larger than experimental error bars

TABLE VI. Parameters of the Vinet EoS (Ref. 30) obtained by least-squares fit of the calculated PAW (P,V) points to which 298 K thermal pressure has been added (values without thermal pressure are given in parentheses). The pressure range of the fit has been chosen equal to the pressure range of available experimental data. Only PAW data sets using semicore states are given within LDA [PW92 (Ref. 20)], GGA-PBE [PBE96 (Ref. 22)] and GGA-PBEsol [PBEsol (Ref. 26)] functionals. The values obtained from experiments (Table IV, Ref. 3 for Pt, Ref. 8 for Au, which includes correction of nonhydrostatic compression effects, and Ref. 15 for ϵ-Fe) have been reported for comparison. The numbers in bold are the closest to experimental values.

Metal		V_0(Å^3)		K_0(GPa)		K_0'	
α-Fe	LDA	10.631	(10.586)	237	(239)	1.88	(1.88)
	GGA-PBE	**11.546**	(11.483)	**181**	(186)	**5.31**	(5.27)
	GGA-PBEsol	10.931	(10.881)	206	(213)	6.56	(6.50)
	Exp.	11.770		165		5.47	
ϵ-Fe	LDA	9.726	(9.697)	329	(334)	4.75	(4.74)
	GGA-PBE	**10.532**	(10.486)	**224**	(229)	**5.46**	(5.44)
	GGA-PBEsol	9.913	(9.880)	297	(301)	4.94	(4.93)
	Exp.	11.214		163		5.38	
Co	LDA	10.124	(10.071)	281	(286)	2.85	(2.84)
	GGA-PBE	**10.992**	(10.914)	**208**	(215)	**4.85**	(4.81)
	GGA-PBEsol	10.542	(10.478)	243	(249)	4.21	(4.18)
	Exp.	11.094		184		4.73	
Ni	LDA	10.099	(10.018)	244	(254)	5.04	(4.99)
	GGA-PBE	**11.008**	(10.893)	**184**	(195)	**5.24**	(5.17)
	GGA-PBEsol	10.477	(10.383)	217	(227)	5.13	(5.08)
	Exp.	10.940		183		4.99	
Zn	LDA	13.805	(13.585)	82	(89)	5.90	(5.80)
	GGA-PBE	**15.760**	(15.365)	**50**	(57)	**6.19**	(6.04)
	GGA-PBEsol	14.468	(14.205)	71	(79)	5.91	(5.80)
	Exp.	15.213		60		5.73	
Mo	LDA	15.145	(15.063)	295	(301)	4.01	(3.99)
	GGA-PBE	15.947	(15.849)	255	(262)	4.17	(4.14)
	GGA-PBEsol	**15.410**	(15.323)	**280**	(287)	**4.05**	(4.02)
	Exp.	15.558		261		4.06	
Ag	LDA	16.178	(16.046)	131	(137)	5.93	(5.87)
	GGA-PBE	18.137	(17.907)	82	(88)	6.23	(6.13)
	GGA-PBEsol	**16.856**	(16.694)	**110**	(116)	**6.05**	(5.98)
	Exp.	17.021		101		5.97	
Pt	LDA	14.898	(14.823)	293	(302)	5.65	(5.61)
	GGA-PBE	15.899	(15.793)	219	(228)	6.20	(6.14)
	GGA-PBEsol	**15.204**	(15.123)	**274**	(282)	**5.64**	(5.60)
	Exp.	15.095		277		5.08	
Au	**LDA**	**16.724**	(16.603)	**187**	(195)	**5.92**	(5.85)
	GGA-PBE	18.173	(17.988)	132	(140)	6.15	(6.07)
	GGA-PBEsol	17.261	(17.122)	169	(176)	5.69	(5.62)
	Exp.	16.962		167		5.88	

for iron, cobalt, nickel, molybdenum, and silver.

In the case of iron, these errors in DFT-GGA-PBE calculated EoS can be due to magnetic effects. DFT calculations[66] have suggested an antiferromagnetic state for ϵ-Fe up to 50 GPa (afmII structure) which has not been clearly evidenced experimentally. Differences between experimental and theoretical EoS at moderate pressures could thus be ascribed to an incorrect modeling of magnetic effects. For other metals, such errors are not expected. No drastic change in the electronic structure of the studied metals was observed on compression. The *d* valence bands become wider, as expected.[69] Numerical and convergence errors can be ruled out here: frozen-core approximation, because inclusion of addition states in valence does not change the EoS; incompleteness of

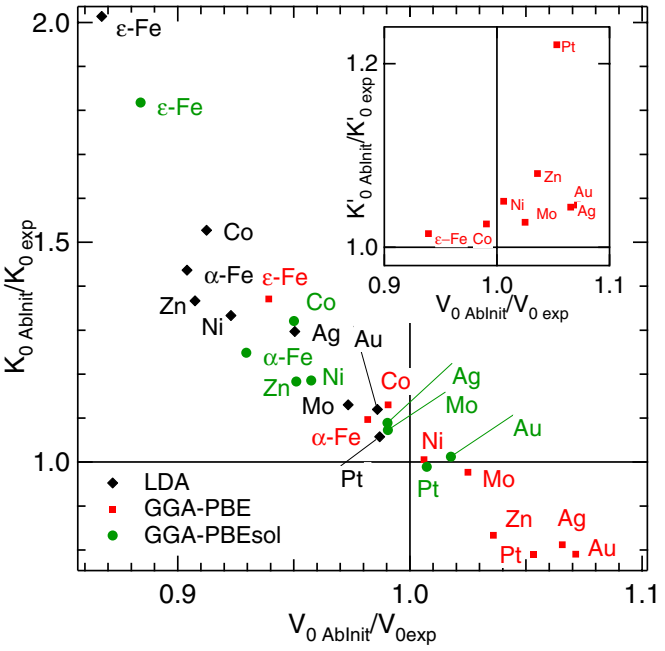

FIG. 5. (Color online) Parameters of Vinet EoS obtained by the PAW method for the studied metals (see Table VI), normalized to the experimental ones. Main graph: normalized bulk modulus vs normalized equilibrium volume obtained with LDA, GGA-PBE and GGA-PBEsol; inset: pressure derivative of the bulk modulus vs normalized volume obtained with GGA-PBE.

PAW partial-wave basis, because FP-LAPW method gives the same results.[70–79] It thus seems likely that the discrepancies between theoretical and experimental EoS are due to the GGA approximation itself. When the functional of Perdew and Wang[20] is used, the exchange energy, which dominates the exchange-correlation term, has been found to be overestimated in absolute value for low electronic densities.[67] Consequently, low densities are nonphysically favored by GGA. That could explain why the bulk modulus becomes overestimated for all metals at high compression, as a resistance of DFT-GGA to stabilize systems with high electronic densities. GGA also favors systems with large electronic gradients compared to LDA;[67] it has recently been suggested that this trend is overestimated in GGA functionals such as PBE96.[26] This is another possible explanation for the inaccuracy of GGA at high compression, which corresponds usually to lower electronic density gradients. LDA becomes a better

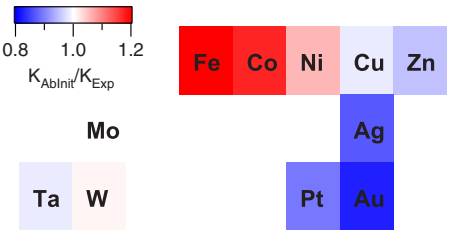

FIG. 6. (Color online) Ratio between the ambient pressure bulk modulus obtained in the GGA-PBE approximation and the experimental one, for the transition metals studied here and in Refs. 3 and 72.

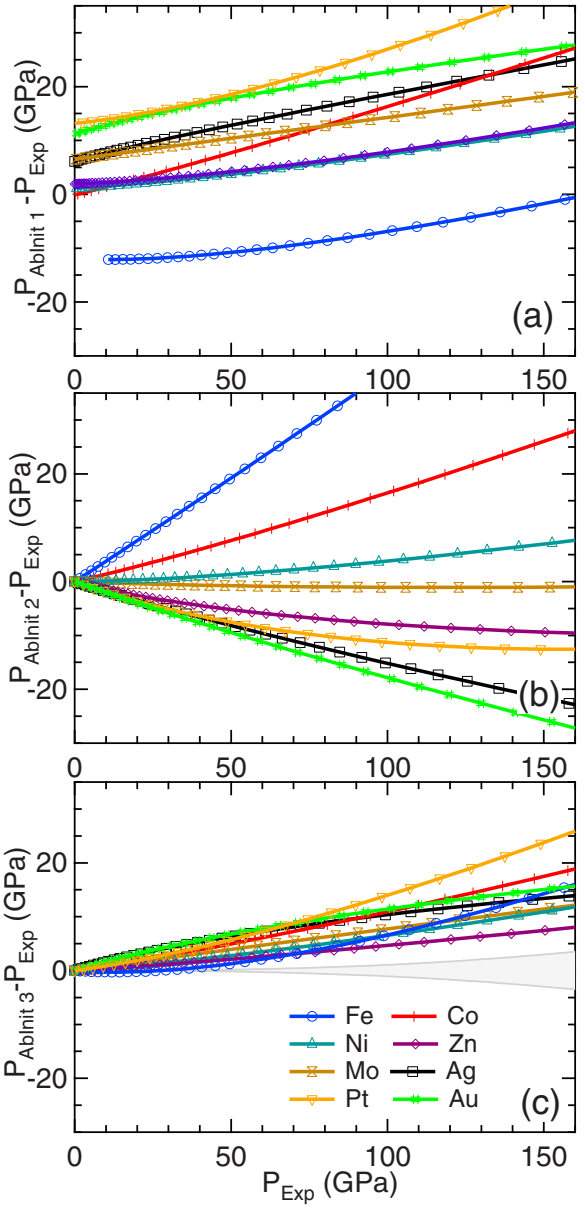

FIG. 7. (Color online) (a) Difference between *ab initio* GGA-PBE pressure $P_{\text{AbInit 1}}$ and experimental pressure P_{exp} for ϵ-Fe, Co, Ni, Zn, Mo, Ag, Pt, and Au. P_{exp} is the Vinet pressure [Eq. (1)] with the following parameters: $(V_{0\,\text{exp}}, K_{0\,\text{exp}}, K'_{0\,\text{exp}})$; $P_{\text{AbInit 1}}$ is calculated using the following parameters: $(V_{0\,\text{AbInit}}, K_{0\,\text{AbInit}}, K'_{0\,\text{AbInit}})$. (b) Same plot, with $P_{\text{AbInit 2}}$ the pressure calculated using Eq. (1) with the following parameters: $(V_{0\,\text{exp}}, K_{0\,\text{AbInit}}, K'_{0\,\text{AbInit}})$. (c) Same plot, with $P_{\text{AbInit 3}}$ the pressure calculated using Eq. (1) with the following parameters: $(V_{0\,\text{exp}}, K_{0\,\text{AbInit Corr}}, K'_{0\,\text{AbInit Corr}})$. The shaded area represents the uncertainty on experimental pressure (see Sec. VI).

approximation for the prediction of the EoS (and hence, the energy) of silver, platinum and gold at high compression.

The present data set evidences that GGA-PBE calculations tend to overestimate the bulk modulus, and thus the pressure, at high compression. This is clearly evidenced in Fig. 7(a), where the difference between *ab initio* GGA and experimental pressures for the same atomic volume is plotted vs the experimental pressure for the metals studied here. For

iron, the ϵ-Fe phase only is considered. Using the present data, we can discuss if GGA-PBE EoS can be corrected in order to reproduce more correctly the experimental EoS. We have thus investigated if a set of Vinet EoS parameters (V_0, K_0, K_0') can be predicted from the output of GGA-PBE calculations, and experimental low-pressure data which are available with a good accuracy for all elements (namely, the volume or the bulk modulus at ambient pressure). It has already been proposed to use experimental V_0 and DFT K_0 and K_0' to generate a high-pressure EoS.[3] The accuracy of this method, for the metals studied here, is illustrated in Fig. 7(b). The difference between the pressure obtained by this method and the experimental pressure is within experimental error bars only for zinc and molybdenum. It reaches 40 GPa and −15 GPa at 100 GPa, respectively, for iron and gold. These high values can be explained by the trend plotted in Fig. 5: The equilibrium volume being respectively underestimated and overestimated for iron and gold, their bulk moduli (and thus GGA-PBE pressure) are thus respectively overestimated and underestimated by more than 10%. We got rid of this bias by generating a Vinet EoS using the following parameters: $(V_{0\ \mathrm{exp}}, K_{0\ \mathrm{AbInit\ Corr}}, K'_{0\ \mathrm{AbInit\ Corr}})$. $K_{0\ \mathrm{AbInit\ Corr}}$ and $K'_{0\ \mathrm{AbInit\ Corr}}$ are, respectively, $K_T(V_{0\ \mathrm{exp}})$ and $K'_T(V_{0\ \mathrm{exp}})$, calculated using the Vinet[30] EoS and GGA-PBE parameters from Table VI. The difference between this EoS and the experimental EoS for the studied metals is plotted in Fig. 7(c). It shows a positive increasing deviation, which is much reduced compared to Figs. 7(a) and 7(b): $P_{\mathrm{AbInit\ 3}} - P_{\mathrm{exp}} = 15.5 \pm 8.0$ GPa at 150 GPa. This difference is decreased by $\simeq 2$ GPa if the new calibration of the ruby gauge proposed in Sec. VI is used, instead of P'_R. However, this method does not appear as a systematic way to correct the errors of DFT and to build an accurate high-pressure EoS from *ab initio* calculations.

VII. CONCLUSIONS

We have presented in this study a joined experimental and theoretical study of the EoS of eight transition metals (iron, cobalt, nickel, copper, zinc, molybdenum, silver, platinum, and gold) in the Mbar range.

Experimental EoS of iron, cobalt, nickel, copper, zinc, molybdenum, and silver have been obtained in a diamond anvil cell, with optimized hydrostatic pressurizing and synchrotron data recording conditions. The recent calibration of the pressure ruby scale has been used. This new experimental determination of the EoS of six metals completes our previous EoS study on six other metals. The calibration of the ruby pressure scale has been verified on this larger data set by the comparison with reduced shock-wave EoS. A marginal difference is obtained but the systematic uncertainty of the ruby pressure scale is now reduced due to improved statistical average.

The EoS of the eight transition metals studied have been calculated using the DFT-PAW method. For that purpose, new atomic data sets suitable for high pressures have been generated. The DFT-PAW EoS are identical to the available all-electron FP-LAPW EoS calculated within the same DFT framework (namely, LDA or GGA with similar functionals).

The detailed comparison between the experiment and calculated determinations of the EoS, homogeneously performed over a set of eight transition metals, enables to quantify and systematize the accuracy of the DFT-LDA/GGA calculations. Three currently used exchange-correlation functionals (LDA, GGA-PBE, GGA-PBEsol) have been implemented. None of these functionals is satisfactory to calculate with more than 20% confidence over the present data set the EoS above 100 GPa. Part of the discrepancy stems from the underestimation or overestimation of the equilibrium volume. However, the increase in bulk modulus with pressure is always overestimated by GGA calculations. A trend of this overestimation of the bulk modulus with the filling of the *d*-orbitals is pointed out. We hope that the present data set will be useful to test new forms of electronic exchange-correlation functionals that would improve the predictability of the DFT calculation of the EoS at high pressure.

ACKNOWLEDGMENTS

The authors acknowledge the European Synchrotron Radiation Facility for provision of synchrotron radiation facilities on beamline ID27. We thank G. Zérah for helpful discussions.

[1] J.-P. Poirier, *Introduction to the Physics of the Earth's Interior* (Cambridge University Press, Cambridge, 1991).
[2] J. D. Lindl, Phys. Plasmas **2**, 3933 (1995).
[3] A. Dewaele, P. Loubeyre, and M. Mezouar, Phys. Rev. B **70**, 094112 (2004).
[4] R. M. Martin, *Electronic Structure: Basic Theory and Practical Methods* (Cambridge University Press, Cambridge, 2004), p. 16.
[5] P. Loubeyre, R. LeToullec, D. Hausermann, M. Hanfland, R. Hemley, H. Mao, and L. Finger, Nature (London) **383**, 702 (1996).
[6] F. Occelli, P. Loubeyre, and R. Letoullec, Nat. Mater. **2**, 151 (2003).
[7] K. Takemura, J. Appl. Phys. **89**, 662 (2001).
[8] A. Dewaele and P. Loubeyre, High Press. Res. **27**, 419 (2007).
[9] M. Mezouar, W. Crichton, S. Bauchau, F. Thurel, H. Witsch, F. Torrecillas, G. Blattmann, P. Marion, Y. Dabin, J. Chavanne, O. Hignette, C. Morawe, and C. Borel, J. Synchrotron Radiat. **12**, 659 (2005).
[10] W. B. Holzapfel, J. Appl. Phys. **93**, 1813 (2003).
[11] K. Kunc, I. Loa, and K. Syassen, Phys. Rev. B **68**, 094107 (2003).
[12] P. I. Dorogokupets and A. R. Oganov, Dokl. Earth Sci. **391A**, 854 (2003).
[13] A. D. Chijioke, W. J. Nellis, A. Soldatov, and I. F. Silvera, J. Appl. Phys. **98**, 114905 (2005).
[14] P. I. Dorogokupets and A. R. Oganov, Phys. Rev. B **75**, 024115

(2007).
[15] A. Dewaele, P. Loubeyre, F. Occelli, M. Mezouar, P. I. Dorogokupets, and M. Torrent, Phys. Rev. Lett. **97**, 215504 (2006).
[16] P. Hohenberg and W. Kohn, Phys. Rev. **136**, B864 (1964).
[17] W. Kohn and L. Sham, Phys. Rev. **140**, A1133 (1965).
[18] D. M. Ceperley and B. J. Alder, Phys. Rev. Lett. **45**, 566 (1980).
[19] J. P. Perdew and A. Zunger, Phys. Rev. B **23**, 5048 (1981).
[20] J. P. Perdew and Y. Wang, Phys. Rev. B **45**, 13244 (1992).
[21] J. P. Perdew and Y. Wang, Phys. Rev. B **33**, 8800 (1986).
[22] J. P. Perdew, K. Burke, and M. Ernzerhof, Phys. Rev. Lett. **77**, 3865 (1996).
[23] P. E. Blochl, Phys. Rev. B **50**, 17953 (1994).
[24] O. K. Andersen, Phys. Rev. B **12**, 3060 (1975).
[25] D. R. Hamann, M. Schlüter, and C. Chiang, Phys. Rev. Lett. **43**, 1494 (1979).
[26] J. P. Perdew, A. Ruzsinszky, G. I. Csonka, O. A. Vydrov, G. E. Scuseria, L. A. Constantin, X. Zhou, and K. Burke, Phys. Rev. Lett. **100**, 136406 (2008).
[27] H.-K. Mao, J. Xu, and P. Bell, J. Geophys. Res. **91**, 4673 (1986).
[28] A. Hammersley, S. Stevenson, M. Hanfland, A. Fitch, and D. Häusermann, High Press. Res. **14**, 235 (1996).
[29] P. M. Bell and H. K. Mao, Year Book - Carnegie Inst. Washington **80**, 404 (1981).
[30] P. Vinet, J. Ferrante, J. Rose, and J. Smith, J. Geophys. Res. **92**, 9319 (1987).
[31] A. Dewaele, F. Datchi, P. Loubeyre, and M. Mezouar, Phys. Rev. B **77**, 094106 (2008).
[32] F. Datchi, A. Dewaele, Y. LeGodec, and P. Loubeyre, Phys. Rev. B **75**, 214104 (2007).
[33] Y. Akahama, H. Kawamura, and A. K. Singh, J. Appl. Phys. **95**, 4767 (2004).
[34] T. S. Duffy, G. Y. Shen, D. L. Heinz, J. F. Shu, Y. Z. Ma, H. K. Mao, R. J. Hemley, and A. K. Singh, Phys. Rev. B **60**, 15063 (1999).
[35] C. S. Yoo, H. Cynn, P. Soderlind, and V. Iota, Phys. Rev. Lett. **84**, 4132 (2000).
[36] N. C. Holmes, J. A. Moriarty, G. R. Gathers, and W. J. Nellis, J. Appl. Phys. **66**, 2962 (1989).
[37] S. N. Vaidya and G. C. Kennedy, J. Phys. Chem. Solids **33**, 1377 (1972).
[38] H.-K. Mao, W. A. Bassett, and T. Takanashi, J. Appl. Phys. **38**, 272 (1967).
[39] K. Takemura, H. Yamawaki, H. Fujihisa, and T. Kikegawa, High Press. Res. **22**, 337 (2002).
[40] K. Takemura (private communication).
[41] R. McQueen, S. Marsh, J. Taylor, J. Fritz, and W. Carter, *High Velocity Impact Phenomenon* (Academic, New York, 1970), Chap. VII.
[42] G. Kennedy and R. Keeler, *American Institute of Physics Handbook*, 3rd ed. (McGraw-Hill, New York, 1972), Chap. 4, pp. 38–105.
[43] R. S. Hixson and J. N. Fritz, J. Appl. Phys. **71**, 1721 (1992).
[44] S. Marsh, *LASL Shock Hugoniot Data* (University of California, Berkeley, 1980).
[45] R. G. McQueen and S. P. Marsh, J. Appl. Phys. **31**, 1253 (1960).
[46] G. Steinle-Neumann, L. Stixrude, and R. E. Cohen, Phys. Rev. B **63**, 054103 (2001).
[47] W. J. Nellis, J. A. Moriarty, A. C. Mitchell, M. Ross, R. G. Dandrea, N. W. Ashcroft, N. C. Holmes, and G. R. Gathers, Phys. Rev. Lett. **60**, 1414 (1988).
[48] A. C. Mitchell and W. J. Nellis, J. Appl. Phys. **52**, 3363 (1981).
[49] N. A. W. Holzwarth, G. E. Matthews, R. B. Dunning, A. R. Tackett, and Y. Zeng, Phys. Rev. B **55**, 2005 (1997).
[50] G. Kresse and D. Joubert, Phys. Rev. B **59**, 1758 (1999).
[51] M. Torrent, F. Jollet, F. Bottin, G. Zerah, and X. Gonze, Comput. Mater. Sci. **42**, 337 (2008).
[52] J. J. Mortensen, L. B. Hansen, and K. W. Jacobsen, Phys. Rev. B **71**, 035109 (2005).
[53] C. Bercegeay and S. Bernard, Phys. Rev. B **72**, 214101 (2005).
[54] D. J. Singh, *Planewaves, Pseudopotentials and the LAPW Method* (Kluwer, Norwell, 1995).
[55] N. Holzwarth, A. Tackett, and G. Matthews, Comput. Phys. Commun. **135**, 329 (2001).
[56] ATOMPAW is a general licence public code developed at Wake Forest University. Some of its capabilites have been developed at the Commissariat à l'Énergie Atomique (http://pwpaw.wfu.edu).
[57] X. Gonze *et al.*, Comput. Mater. Sci. **25**, 478 (2002).
[58] G.-M. R. X. Gonze *et al.*, Z. Kristallogr. **220**, 558 (2005).
[59] The ABINIT code is a common project of the Université Catholique de Louvain, Corning Incorporated, the Commissariat à l'Energie Atomique, the Université de Liège, Mitsubishi Chemical Corp. and other contributors (http://www.abinit.org).
[60] M. Verstraete and X. Gonze, Phys. Rev. B **65**, 035111 (2001).
[61] D. E. Gray, *American Institute of Physics Handbook*, 2nd ed. (McGraw-Hill, New York, 1963).
[62] J. Xie, S. P. Chen, H. V. Brand, and D. L. Rabie, J. Phys.: Condens. Matter **12**, 8953 (2000).
[63] J. Xie, S. P. Chen, S. D. Gironcoli, and S. Baroni, Philos. Mag. B **79**, 911 (1999).
[64] O. Anderson, D. Isaak, and S. Yamamoto, J. Appl. Phys. **65**, 1534 (1989).
[65] A. B. Alchagirov, J. P. Perdew, J. C. Boettger, R. C. Albers, and C. Fiolhais, Phys. Rev. B **63**, 224115 (2001).
[66] G. Steinle-Neumann, L. Stixrude, and R. E. Cohen, Phys. Rev. B **60**, 791 (1999).
[67] J. P. Perdew, J. A. Chevary, S. H. Vosko, K. A. Jackson, M. R. Pederson, D. J. Singh, and C. Fiolhais, Phys. Rev. B **46**, 6671 (1992).
[68] V. Ozolins and M. Körling, Phys. Rev. B **48**, 18304 (1993).
[69] T. Tsuchiya and K. Kawamura, Phys. Rev. B **66**, 094115 (2002).
[70] F. Jona and P. M. Marcus, J. Phys.: Condens. Matter **17**, 1049 (2005).
[71] A. Khein, D. J. Singh, and C. J. Umrigar, Phys. Rev. B **51**, 4105 (1995).
[72] Y. Wang, D. Chen, and X. Zhang, Phys. Rev. Lett. **84**, 3220 (2000).
[73] P. Loubeyre, R. LeToullec, M. Hanfland, L. Ulivi, F. Datchi, and D. Hausermann, Phys. Rev. B **57**, 10403 (1998).
[74] N. W. Guinan and D. N. Beshers, J. Phys. Chem. Solids **29**, 541 (1968).
[75] G. Simmons and H. Wang, *Single Crystal Elastic Constants and Calculated Aggregate Properties: A Handbook* (MIT, Cambridge, MA, 1971).
[76] M. Yamamoto, Phys. Rev. **77**, 566 (1950).
[77] H. M. Ledbetter, J. Phys. Chem. Ref. Data **6**, 1181 (1977).
[78] K. W. Katahara, M. H. Mangnani, and E. S. Fisher, J. Phys. F: Met. Phys. **9**, 773 (1979).
[79] W. Holzapfel, M. Hartwig, and W. Sievers, J. Phys. Chem. Ref. Data **30**, 515 (2001).